

Cover Page



Universiteit Leiden



The handle <http://hdl.handle.net/1887/25579> holds various files of this Leiden University dissertation

Author: Driessen, R. P. C.

Title: The architects of crenarchaeal chromatin : a biophysical characterization of chromatin proteins from *Sulfolobus solfataricus*

Issue Date: 2014-05-06

CHAPTER 2

Crenarchaeal chromatin proteins Cren7 and Sul7 compact DNA by inducing rigid bends

This chapter has been published as:

Rosalie P.C. Driessen, He Meng, Gorle Suresh, Rajesh Shahapure, Giovanni Lanzani, U Deva Priyakumar, Malcolm F. White, Helmut Schiessel, John van Noort and Remus Th. Dame, *Nucleic Acids Research*, **41**, 196-205, 2013

ABSTRACT

Archaeal chromatin proteins share molecular and functional similarities with both bacterial and eukaryotic chromatin proteins. These proteins play an important role in functionally organizing the genomic DNA into a compact nucleoid. Cren7 and Sul7 are two crenarchaeal nucleoid-associated proteins, which are structurally homologous, but not conserved at the sequence level. Co-crystal structures have shown that these two proteins induce a sharp bend on binding to DNA. In this study, we have investigated the architectural properties of these proteins using atomic force microscopy, molecular dynamics simulations and magnetic tweezers. We demonstrate that Cren7 and Sul7 both compact DNA molecules to a similar extent. Using a theoretical model, we quantify the number of individual proteins bound to the DNA as a function of protein concentration and show that forces up to 3.5 pN do not affect this binding. Moreover, we investigate the flexibility of the bending angle induced by Cren7 and Sul7 and show that the protein–DNA complexes differ in flexibility from analogous bacterial and eukaryotic DNA-bending proteins.

INTRODUCTION

Organisms in all three domains of life need to compact and functionally organize their genomic DNA into the relatively small volume of a nucleus or a cell. Architectural proteins (histones and other chromatin proteins in eukaryotes and nucleoid-associated proteins in bacteria and archaea) play an important role both in compaction and functional organization of DNA, thus affecting DNA transactions as diverse as transcription, repair and replication (14).

In eukaryotes, DNA is wrapped around histone octamers, forming nucleosomes. With the aid of other chromatin proteins, fibres with nucleosomes are folded into higher-order structures, obtaining multiple levels of organization. Bacteria organize their genomic DNA into a nucleoid, which is shaped by the action of small chromatin proteins that bend or bridge the DNA (e.g. HU, IHF, Fis and H-NS) (36,37). Archaea, constituting the third domain of life, synthesize numerous nucleoid-associated proteins with molecular and functional similarities to both bacterial and eukaryotic chromatin proteins (39,183). The two main archaeal phyla, Euryarchaea and Crenarchaea, express different sets of chromatin proteins, none of which is conserved throughout the whole archaeal domain. Euryarchaea synthesize true tetrameric histone homologues, which form nucleosomes similar to eukaryotic tetrasomes (44,45). Crenarchaea, on the other hand, do not synthesize histone homologues, although there are some rare exceptions (184). Each crenarchaeal species encodes at least two different small chromatin proteins and several paralogues, which may act in concert to compact the genomic DNA and to regulate its accessibility (40).

In the crenarchaeum *S. solfataricus*, four nucleoid-associated proteins have been identified so far, Alba, Sso10a, Cren7 and Sso7d (the Sul7 family of chromatin proteins). Alba forms dimers in solution (71) and has been shown to bridge DNA at low concentrations, providing a means of organizing and compacting DNA (81,178). Sso10a homologues (65,109) also

exist as dimers in solution and have been shown to form protein-DNA complexes, similar in appearance to Alba-DNA complexes (81). Otherwise, little is known about the role of Sso10a in compacting and organizing genomic DNA.

Cren7 and Sul7 are both small (~ 7 kDa) basic monomeric proteins, which bind to DNA with no apparent sequence specificity. Although they share no similarities at the amino acid level, their tertiary structures and their biochemical properties are very similar (61-63,92-94,105). Both proteins are folded similarly, containing two antiparallel β -sheets. They mainly differ in the presence of an extended loop located in between the two β -sheets in Cren7 (63) and an additional C-terminal α -helix in Sul7 (70). Protein-DNA co-crystal structures showed that they bind to DNA by intercalation of hydrophobic side chains into the minor groove (see inset Figure 2.1), which results in bending of DNA by up to $50 - 60^\circ$ (95-97,100,101).

The transcriptome of *S. solfataricus* P2 shows high levels of transcription of both Cren7 and Sul7 (110), and, consequently, both proteins are abundant in the cell (~ 1% and up to 5% of the total cellular protein for Cren7 and Sul7 respectively (63,92)). Native Cren7 and Sul7 proteins are post-translationally modified by methylation of several lysine residues. Nevertheless, the function of methylation remains unclear, as it does not change the binding affinity to DNA *in vitro* (62,63), in contrast with the acetylation of Alba (167).

Proteins that bend DNA by sequence non-specific binding into the minor groove play an important role in DNA compaction and chromatin organization throughout all domains of life (14,185-188). In eukaryotes, high-mobility group (HMG) proteins form moderately flexible bends in DNA by intercalating into the minor groove (188), enhancing the overall flexibility of the DNA, and they are likely to play a supplementary role in chromatin organization (187). In bacteria, DNA-bending proteins are crucial players in chromatin organization, as bacteria lack histone homologues.

That Cren7 and Sul7 function similarly to this group of bacterial and eukaryotic DNA-bending proteins is suggested by the co-crystal structures, but has not yet been investigated. A functional difference between the two proteins is expected as they coexist in species from the Sulfolobales order, but previously reported biochemical assays have not yet revealed a significant difference in protein-DNA interactions between Cren7 and Sul7. To obtain a detailed understanding of the architectural properties of the two proteins, we use a set of different techniques including atomic force microscopy (AFM), molecular dynamics (MD) simulations and magnetic tweezers. Our AFM studies yield insight in the overall compaction properties of the two proteins. The MD simulations using X-ray co-crystal structures yield an ensemble of equilibrated ‘solution conformations’ of the complexes. This gives information on the DNA bending angle induced and the rigidity of this bend. With magnetic tweezers we investigate the mechanical properties of single protein-DNA complexes. Elaborate analysis of measured force-extension curves enables us to quantify the number of proteins bound on single DNA molecules and to get a detailed understanding on the force-dependency of protein binding and the flexibility of the bending angle.

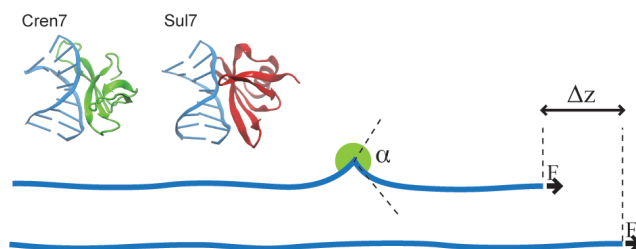


Figure 2.1 Schematic illustrating the reduction of end-to-end distance due to binding of a DNA-bending protein. Binding of a protein that induces a bend of deflection angle α reduces the end-to-end distance with $\Delta z = -1/2 \cdot \lambda \cdot C(\alpha)$. Inset: Average conformation of the Cren7-DNA and Sul7-DNA complexes obtained from MD simulations. Both proteins bend the DNA by intercalating in the minor groove. Images are generated using visual molecular dynamics (VMD) software (189).

RESULTS AND DISCUSSION

To investigate the architectural properties of Cren7 and Sul7, we used a combination of different single-molecule techniques. We used AFM to visualize individual protein-DNA complexes, MD simulations to evaluate the bending angle of the protein-DNA complexes in solution and magnetic tweezers experiments to quantify the physical properties of single protein-DNA complexes and their force dependency.

Effect of Cren7 and Sul7 on the conformation of single DNA molecules

To investigate the effect of Cren7 and Sul7 on the conformation of single DNA molecules, we visualized protein-DNA complexes using AFM. As can be seen in Figure 2.2, addition of either Cren7 or Sul7 results in DNA conformations that are more compact than bare DNA molecules. An increasing amount of protein results in a higher degree of compaction. It is likely that the observed compaction is caused by bends induced by the proteins. However, the small size of the proteins (~ 7 kDa) limits the unambiguous identification and quantitative analysis of individual proteins on the DNA. To gain more insights into the structure and dynamics of the bends induced by the two proteins, we carried out MD simulations of protein-DNA complexes in solution.

Bending angle determination by MD simulations

The co-crystal structures of Cren7-DNA and Sul7-DNA complexes showed that both proteins induce a bending in the DNA of $\sim 50 - 60^\circ$. However, a complex in a crystal is fixed in a single conformation and may reflect a rare conformation favoured by crystal packing. To evaluate whether the bending angles observed in the co-crystal structures reflect the average conformation in solution, we performed MD simulations in solution using the co-crystal structures as initial coordinates. The MD simulations yielded stable structures except for a small deviation in the Sul7-DNA complex at the end

of the simulation run because of rigid body motions of the C-terminal region (see Figure S2.1 for the root mean square deviations). The overall flexibility of the DNA in all three complexes examined using root mean square deviations was found to be similar. Additionally, the extent of DNA bending was investigated by calculating the roll angle (ρ). Figure 2.3 shows the probability distributions of the roll angles during the simulation. Fitting the distributions to a Gaussian we find that both protein-DNA complexes exhibit similar bending angles of $\alpha_{\text{Cren7}} = 47.5 \pm 5.6^\circ$ and $\alpha_{\text{Sul7}} = 45.3 \pm 6.7^\circ$, which slightly deviate from the bending angle found in the co-crystal structures. It is important to note that the width of the roll angle distributions (which reflects the flexibility of the complex) of both protein-DNA complexes is small and comparable with the width of the roll angle distribution of bare DNA ($\alpha_{\text{bareDNA}} = 7.3 \pm 5.7^\circ$).

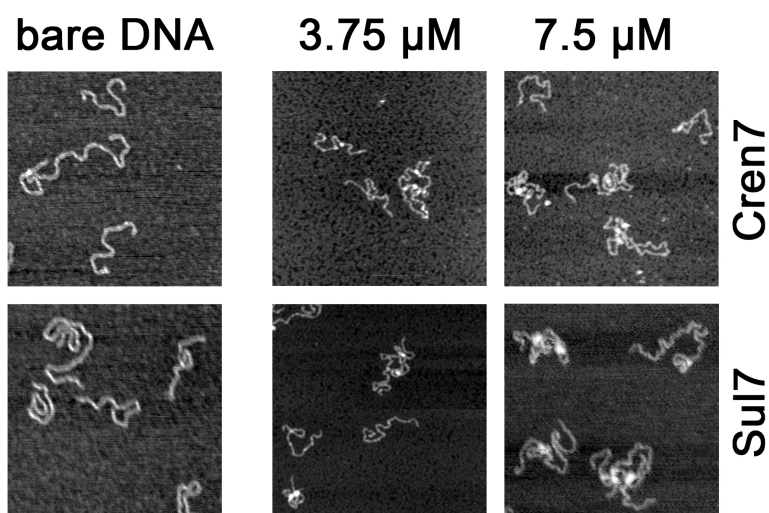


Figure 2.2 AFM images of bare DNA, Cren7-DNA complexes and Sul7-DNA complexes. The protein-DNA complexes are more compact than the bare DNA molecules. Increasing the protein concentration results in more compaction. The DNA is an equimolar mixture of both 1841 and 845 bp linear fragments. Images are 500 x 500 nm in size.

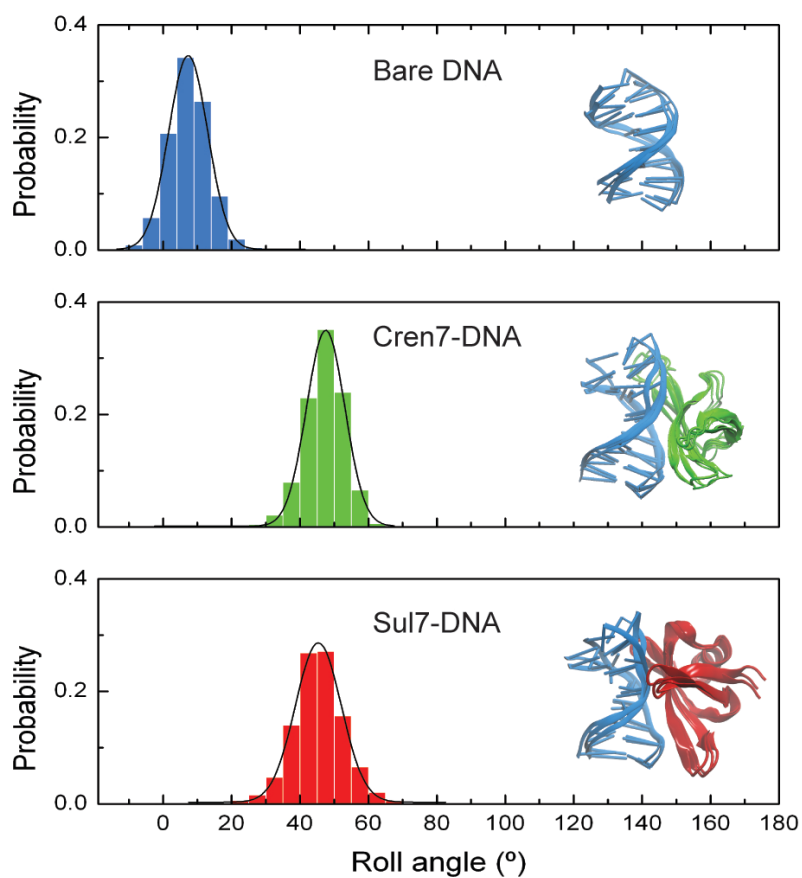


Figure 2.3 Probability distribution of the roll angle of the kinked base pair step in the bare DNA (*blue*), the DNA in the Cren7-DNA complex (*green*) and the DNA in the Sul7-DNA complex (*red*). Distributions are obtained from the final 90 ns of the MD simulations and fitted to a Gaussian ($\alpha_{\text{bareDNA}} = 7.3 \pm 5.7^\circ$, $\alpha_{\text{Cren7}} = 47.5 \pm 5.6^\circ$ and $\alpha_{\text{Sul7}} = 45.3 \pm 6.7^\circ$). Insets: The average conformations of the bare DNA the Cren7-DNA and Sul7-DNA complexes are shown and aligned with two extreme conformations to illustrate the flexibility of the complexes. Images are generated using visual molecular dynamics (VMD) software (189).

Quantification of DNA compaction by Cren7 and Sul7

To quantify the molecular mechanisms underlying the observed DNA compaction, we carried out single-molecule micromanipulation experiments. In these experiments, we measured the force-extension relation of single double stranded DNA (dsDNA) molecules over a range of concentrations for both Cren7 and Sul7 (0, 40, 80, 200, 400 and 800 nM) (Figure 2.4 A and B). In both cases, the addition of protein results in a reduction of z (compaction), which decreases progressively upon raising the protein concentration. No significant difference is observed between Cren7 and Sul7 as they compact the DNA to a similar extent, which confirms the compaction observed in our AFM studies. The reduction of the end-to-end distance (z) saturates at a protein concentration of ~ 400 nM (Figure 2.4 C and D). At the highest concentration (800 nM), the end-to-end distance increases slightly, which could point to interactions between adjacent proteins, causing a mild extension of the compacted DNA molecules. However, incubation with higher protein concentrations (up to 1600 nM) did not induce a further increase in end-to-end distance (*data not shown*).

To quantify the effects of the protein on the mechanical properties of DNA, the WLC model [Equation (2.2)] was fitted to the force-extension curves. While the contour length stays constant ($L_0 = 1.0 \pm 0.05 \mu\text{m}$), the apparent persistence length ($l_{p,192}$) decreases drastically (Figure 2.5). At high concentrations the apparent persistence length reaches a minimum of $L_p = 8.8 \pm 1.3$ nm for Cren7 and $L_p = 9.0 \pm 1.6$ nm for Sul7, which is more than four times smaller than the measured persistence length of bare DNA, $L_p = 40.5 \pm 11.2$ nm. Thus, binding of these proteins results in compaction of DNA by reducing the apparent persistence length.

It is interesting to note that higher protein concentrations do not result in stiffening of the DNA. Previous studies of similar DNA-bending proteins (e.g. the bacterial proteins HU and IHF and eukaryotic HMG proteins) have shown that these proteins compact DNA by forming bends at low protein

concentrations (193-196). However, HU and HMG proteins enter a second binding regime at high concentrations, forming stiff filaments due to close adjacent binding. It has been suggested that IHF behaves similarly (37) when binding non-specifically along DNA (193,197), but this has not yet been experimentally confirmed. The bimodal binding of HU, causing a transition from a softening to a stiffening mode, has been shown to be salt dependent and was only observed at NaCl concentrations < 150 mM (198).

As such salt-dependent effects might exist also for Cren7 and Sul7, we measured force-extension curves under different ionic conditions. Previous studies have already shown that the binding affinity of Sul7 decreases with increasing ionic strength (199). Measurements in a buffer containing a lower salt concentration (25 mM NaCl) showed that the decrease in apparent persistence length occurs at much lower protein concentration (Figure 2.5 B), which suggests an increased binding affinity, because of enhanced electrostatic protein-DNA interactions at low ionic strength, as expected. Again at the highest protein concentration the persistence length did not increase and a stiffening mode was not observed. These findings suggest that Cren7 and Sul7 do not stiffen DNA in a second binding mode, even at protein concentrations where high DNA coverage is expected. It has been shown for bacterial H-NS-like proteins that these proteins exhibit two binding modes (116,200,201), which can be switched by the addition of $MgCl_2$ (115,202). To test whether divalent ions have an effect on the mode of binding of Cren7 and Sul7 we performed measurements in the presence of $MgCl_2$. These experiments did not reveal an effect on the binding behaviour of Cren7 and Sul7, other than a decrease in binding affinity (see Figure S2.2). This reinforces that the binding is dominated by electrostatic interactions, which are reduced by increasing the ionic strength.

Quantification of the number of proteins bound

The number of proteins bound to the DNA within the range of measured force and protein concentrations is determined by applying Equation (2.5) to

the measured force-extension curves (Figure 2.4 A and B) using the bending angle α determined from the MD simulations ($\alpha_{\text{Cren7}} = 47.5^\circ$ and $\alpha_{\text{Sul7}} = 45.3^\circ$, see Figure 2.3). As expected, the number of proteins bound on the DNA (N_b) increases with increasing protein concentration (see Figure 2.6).

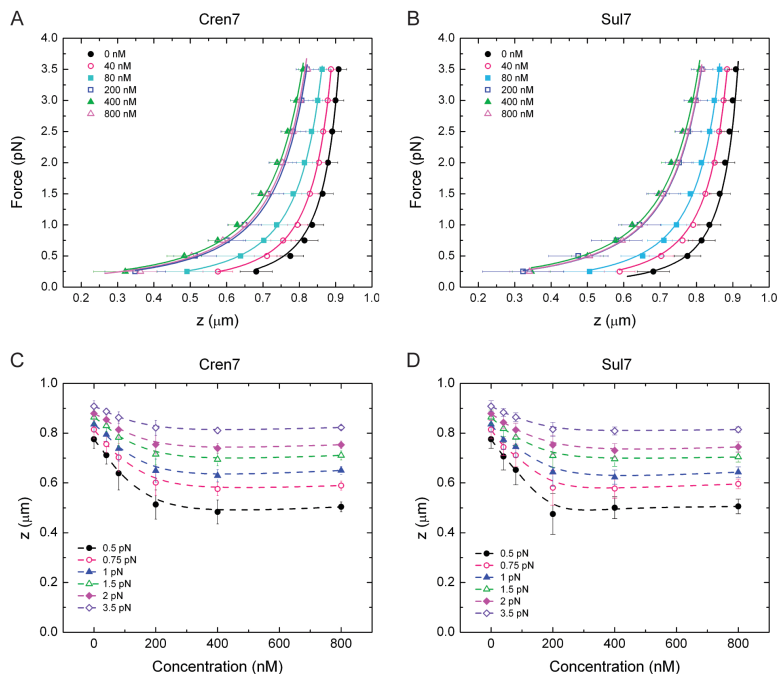


Figure 2.4 Force-extension curves of protein-DNA complexes. Each data point represents the average of a number of DNA molecules measured in buffer containing 100 mM NaCl ($N = 26$ for bare DNA molecules and $N = 6 - 14$ for DNA-protein complexes). Data is fitted with the WLC model [Equation (2.2)]. Error bars represent the standard deviation. **A and B.** Averaged force-extension curves of DNA at different protein concentrations of Cren7 and Sul7. **C and D.** End-to-end distance as a function of bulk protein concentration represented at constant forces. Progressive addition of protein results in a decrease of the end-to-end distance z , and thus compaction of DNA molecules.

Considering the condition for which our model is valid $N_b \ll L_0 / \lambda$ (see Materials and Methods section), we note that this condition holds for the 40 nM and 80 nM measurements, where proteins are still bound distant enough from each other. For the lowest concentrations the number of bound proteins is found to be constant throughout the measured force range (Figure 2.6), from which we conclude that forces up to 3.5 pN do not affect the number of proteins on the DNA. At higher protein concentrations, the high occupancy may introduce a systematic error in the calculated N_b , but as in the case of lower concentrations we still find a force independent value for N_b .

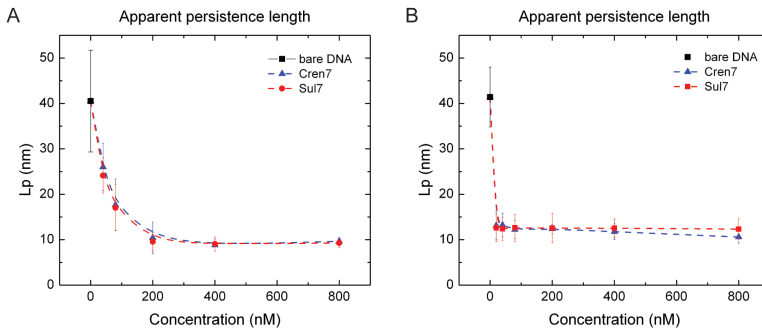


Figure 2.5 Apparent persistence length (L_p) decreases as a function of protein concentration. The persistence length is determined by fitting individual force-extension curves to the WLC model [Equation (2.2)] and averaged for each concentration point. Error bars represent the standard deviation. **A.** Average apparent persistence length from F-z curves measured in buffer containing 100 mM NaCl. **B.** Average apparent persistence length from F-z curves measured in buffer containing 25 mM NaCl.

This is a surprising observation, as one would expect a significant decrease in binding affinity with applied force. The energy it costs to form a bend is force-dependent and for the highest force (3.5 pN) this would be $E_{\text{kink}} = \sim k_B T$ (see Supplementary Information). As the dissociation constant K_d is related to E_{kink} and the binding free energy ΔG_0 as follows:

$$K_d(F) \sim \exp\left(\frac{\Delta G_0 + E_{kink}(F)}{k_B T}\right) \quad (2.1)$$

one would expect the dissociation constant to increase with a factor 2.7 for both Cren7 and Sul7 when the force is increased from 0 to 3.5 pN, resulting in a lower protein occupancy at higher forces. Apparently, these proteins bind stably enough to withstand such forces on our experimental timescale (~ 30 s). Note that measurements were reversible for all measured protein concentrations, which could be explained by off-rates much larger than the experimental timeframe (see Figure S2.3). Even holding the protein-DNA complexes at 3.5 pN for 10 minutes did not result in an increase in z or a different retraction curve showing that the proteins stay stably bound even on longer timescales (see Figure S2.4). Unexpectedly, low off-rates of proteins bound to DNA have also been observed in previous studies on HU and HMG protein-DNA complexes in protein free solution (198,203). Apparently, there is a large energy barrier for the proteins to dissociate which is not reached by applying a force of 3.5 pN. Such strong binding could be crucial for maintaining the integrity of the DNA in extreme environmental conditions of the organism's natural habitat. Cellular processes that apply local tension on the DNA such as transcription, replication and repair act on timescales that are much shorter compared with our experimental timescale. This suggests that these proteins are relatively stably bound to the DNA *in vivo*. However, cellular machineries involved in replication and transcription such as helicases and polymerases may directly drive the proteins to dissociate (204) allowing access to the DNA track.

Determining the number of proteins bound to DNA and how this is affected by force on the DNA has been a topic of interest in various recent studies (205-208). It is important in the light of understanding the contribution of the individual bound proteins to overall genome organization and how forces induced by cellular processes affect this.

Theoretical models have described the number of proteins bound to single DNA molecules in relation to applied force. These models showed that the force response of the bound proteins is highly dependent on the flexibility of the protein-DNA complex if the binding is relatively strong (207). With the use of thermodynamic Maxwell relations (208), the change in the number of bound proteins can be determined, given the condition that the protein-DNA interactions are in thermodynamic equilibrium. Analysis with the thermodynamic Maxwell relations of single-DNA force-extension data with DNA-bending proteins from *E. coli*, HU and Fis, suggested that these proteins are driven off the DNA by an applied force, even at relatively small forces < 1 pN (206). It should be noted, however, that this approach does not take into account that the degree of protein induced DNA bending could be altered by DNA tension. Applying force to the protein-DNA complexes could reduce the degree of bending, which would result in a net mechanical response, similar to that of protein unbinding (196). Thus, the proposed unbinding of proteins in those studies might actually be (in part) caused by a decrease of bending angle rather than protein unbinding.

Do Cren7 and Sul7 induce flexible or static bends?

Previous studies of bacterial chromatin protein HU have shown that bends of HU-DNA complexes are highly flexible (209) [varying from 0° to 180° (210)]. Although a similar flexible hinge model was initially proposed for eukaryotic HMG domains (194), further experiments showed a more narrow angle distribution of HMGB-DNA complexes (188). Non-specific binding of IHF may induce flexible bends analogous to HU, whereas the site-specific binding of IHF is stabilized by interaction between the DNA flanking the kink sites and the body of the protein, making this bend static (209). Based on the analogy of Cren7 and Sul7 with those non-specific DNA-bending proteins, one would anticipate that these proteins induce bends with a certain degree of flexibility. Applying a force on such flexible bends would decrease the bending angle. Equation (2.5) yields an increase of the extension of the DNA for both a reduction in the bending angle and a

reduction of N_b , which are indistinguishable from each other. Surprisingly, the number of bound proteins N_b is unaffected by the applied force, which implies that the bending angles are independent of forces ≤ 3.5 pN. The MD simulations of the protein-DNA complexes in solution at zero force show that the distributions of roll angles are narrow (Figure 2.3) ($\alpha_{\text{Cren7}} = 47.5 \pm 5.6^\circ$ and $\alpha_{\text{Sul7}} = 45.3 \pm 6.7^\circ$) and comparable in width with the roll angle distribution of bare DNA ($\alpha_{\text{bareDNA}} = 7.3 \pm 5.7^\circ$). Both observations show that Cren7 and Sul7 bind with a rigid bend, in contrast with flexible hinges induced by analogous DNA-bending proteins. If a flexible angle is essential in permitting tight packing of proteins this could explain the absence of a second binding mode in which the DNA is stiffened.

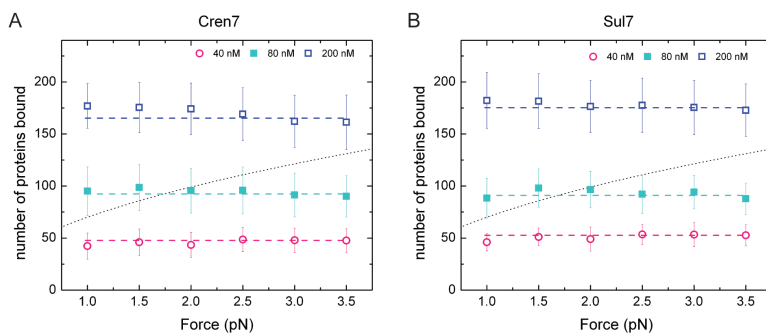


Figure 2.6 Number of bound proteins (N_b) on a single DNA molecule (2947 bp) as a function of force, calculated from the force-extension curves according to Equation (2.5). The number of proteins increases with increasing protein concentration, but is unaffected by forces up to 3.5 pN. Lines represent N_b calculated from the apparent persistence length. Black dashed line represents the condition $N_b \ll L_0 / \lambda$.

CONCLUSIONS

The protein-DNA interactions of Cren7 and Sul7 are very similar. Like in previous biochemical assays we found that they bind with comparable affinity. Here we have demonstrated that they induce a similar degree of

compaction of DNA, bind independent of forces up to 3.5 pN and bend DNA with a non-flexible bend. Whether the bending and binding of Cren7 and Sul7 also resists higher forces remains to be seen and could be assessed with other single-molecule techniques that permit DNA-stretching at higher forces. Visualization of fluorescent proteins in combination with such techniques (211) could confirm our findings in the low force regime. Although no difference has yet been observed, given the fact that Cren7 and Sul7 coexist in the same organisms one would still expect them to have a functional difference *in vivo*. As mentioned earlier, Cren7 and Sul7 can both be methylated at several lysine residues. Such post-translational modifications of nucleoid-associated proteins can play an important role in regulation of interactions between individual proteins on the DNA, as well as the interaction with other proteins, such as transcription factors or other chromatin proteins. How this affects the role of Cren7 and Sul7 in chromatin organization, and possibly gene regulation, remains to be investigated.

MATERIALS AND METHODS

Protein purification

Cren7

The Cren7 protein was purified from *Escherichia coli* strain BL21 (DE3) containing plasmid pET30a, including the gene encoding Cren7 (gene SSO6901) from *S. solfataricus* (63). Cells were grown in LB medium up to $OD_{600} \approx 0.4$ and expression was induced using 0.5 mM IPTG at 37 °C. Two hours after induction, cells were harvested by centrifugation, washed with physiological saline (0.9% w/v NaCl), and resuspended in buffer A [50 mM Tris-HCl (pH 8.0), 10 mM ethylenediaminetetraacetic acid (EDTA), 10% Glycerol, 10 mM β -mercaptoethanol]. Cells were lysed by sonication, and the cell lysate was centrifuged at 37,000 r.p.m. for 30 min at 4°C. The supernatant was applied to an SP column (GE Healthcare) and was eluted with buffer A containing 200 mM NaCl. The eluted protein was heated at

65 °C for 30 min and centrifuged at 37.000 r.p.m. for 15 min. The supernatant was diluted to 100 mM NaCl in buffer A, loaded on a heparin column (GE Healthcare) and eluted with a linear gradient of 0.1 – 1 M NaCl in buffer A. The protein was eluted at ~ 270 mM NaCl.

Sul7

A synthetic gene encoding the *S. solfataricus* Sul7 (Sso7d) protein (gene SSO10610) was constructed in expression vector pJexpress411 (supplied by DNA2.0). The DNA sequence used is available from the authors on request. The plasmid was transformed into *E. coli* strain BL21 (DE3) Rosetta cells, grown in LB medium, and expression was induced using 0.2 mM IPTG at 37 °C for 3 h. Following cell lysis by sonication, the Sul7 protein was loaded onto a heparin column (GE Healthcare) and eluted with a linear gradient of 0 – 1 M NaCl in buffer B [20 mM Tris-HCl (pH 7.4), 1 mM DTT, 1 mM EDTA]. Fractions containing the Sul7 protein were pooled, concentrated and applied to a Superdex 200 gel filtration column (GE Healthcare) and were eluted by isocratic flow with buffer B supplemented with 200 mM NaCl.

Cren7 and Sul7 proteins were dialysed at 4 °C against a storage buffer [20 mM Hepes (pH 7.5), 100mM NaCl, 10% Glycerol, 10 mM β -mercaptoethanol], and stored at -80 °C until required. Protein concentrations were determined by ultraviolet absorbance at 280 nm, using a molar extinction coefficient $\epsilon_{\text{Cren7}} = 8250 \text{ M}^{-1}\text{cm}^{-1}$ (63) and $\epsilon_{\text{Sul7}} = 8300 \text{ M}^{-1}\text{cm}^{-1}$ (70).

DNA constructs

AFM

pUC18 was propagated in *E. coli* strain XL10 and was purified (Qiagen plasmid midi kit). Digestion with EcoRI and XmnI resulted in a mixture of 845-bp and 1841-bp linear fragments.

Magnetic tweezers

pBluescript II KS+ (Stratagene) was digested with Sall and HindIII enzymes to generate a 2947-bp linear fragment. The cohesive end at the Sall digestion site was labelled with dUTP-digoxigenin (DIG), using the Klenow fragment (Fermentas). Subsequently the fragments were purified, labelled with dUTP-biotin at the extremity resulting from HindIII digestion using dATP, dCTP and dGTP and the Klenow fragment and were purified again.

Molecular dynamics simulations

MD simulations of 100 ns were performed in an explicit solvent environment as previously described (103) using initial coordinates from the co-crystal structures of Cren7-DNA and Sul7-DNA (PDB codes 3LWH and 1BNZ respectively) and an ideal B-DNA duplex with identical sequence was used for the bare DNA simulation. A detailed description can be found in the supplementary materials and methods (see Supplementary Information).

Atomic Force Microscopy experiments

Freshly cleaved mica was incubated with 10 μ l of 0.05% poly-L-lysine, rinsed with MilliQ water and dried with nitrogen gas. Protein-DNA complexes were formed by incubating 50 ng of DNA with varying concentrations of protein in 10 μ l buffer containing 10 mM HEPES (pH 7.5) and 100 mM NaCl for 10 min at room temperature (\sim 23 $^{\circ}$ C). After incubation, this mixture was diluted 5-fold in water and was directly deposited onto poly-L-lysine coated mica, rinsed with MilliQ water and dried with nitrogen gas. Images were collected on a NanoScopeIII AFM (Digital Instruments, Santa Barbara, CA) using tapping mode in air (micro cantilevers, Olympus MCL-AC240TS-W2, resonance frequency 70 kHz, spring constant 2 N/m) at a frequency of 2 Hz and were flattened using Nanoscope software (Veeco Instruments).

Magnetic tweezers experiments

Magnetic tweezers experiments were performed on a custom-built instrument described earlier (212). Images were acquired with a CCD camera (Pulnix TM-6710CL) at 60 Hz and real time image processing was done using custom-developed LabView software (National Instruments). Magnets were positioned in the optical axis of the microscope and were controlled by a stepper motor-based translational stage (M-126, Physik Instrumente). Force was calibrated by measuring fluctuations of a tethered DNA-bead construct and was calculated according to the equipartition theorem (213).

The bottom slide of the flow cell was pre-coated with 1% (w/v) polystyrene in toluene. Subsequently, the flow cell was filled with 1 $\mu\text{g/ml}$ anti-DIG antibodies (Roche) and was incubated for 2 h at 4 °C. Next, the flow cell was flushed with 2% (w/v) bovine serum albumine (BSA) and 1% (v/v) Tween-20 solution and was incubated overnight at 4 °C. The flow cell was flushed with buffer I [10 mM HEPES (pH 7.6), 100 mM KAc, 0.2% (w/v) BSA, 0.1% (v/v) Tween-20], filled with 20 ng/ml DNA (functionalized with biotin and DIG) in buffer I and incubated for 10 min. One microlitre of streptavidin coated superparamagnetic beads with a diameter of 1 μm (DYNAL Myone) was washed three times in 1x TE [10 mM Tris-HCl (pH 8.0), 1 mM EDTA], resuspended in 500 μl buffer I, flushed into the flow cell and incubated for 10 minutes. Before measurements, the flow cell was washed thoroughly (~ 10 times the volume of a flowcell) with buffer II [10 mM HEPES (pH 7.5), 0.2% (w/v) BSA, 0.1% (v/v) Tween-20] with addition of either 25 mM or 100 mM NaCl (with or without 10 mM MgCl_2 added). Cren7 and Sul7 stock solutions were diluted in buffer II to the desired protein concentration (40 – 800 nM), and incubated for 10 minutes before starting measurements. Force-extension curves of single double-stranded DNA (dsDNA) molecules and protein-DNA complexes were measured by increasing the force to 3.5 pN during 30 s and subsequently reducing the

force to zero in 10 s. All measurements were performed at room temperature (~ 23 °C).

Data analysis

Force-extension curves of single dsDNA molecules and protein-DNA complexes were quantified using the worm-like chain model (WLC). This model describes the mechanical properties of DNA and is defined by its intrinsic properties: the persistence length L_p and the contour length L_0 (214):

$$F(z) = \left(\frac{k_B T}{L_p} \right) \left(\frac{1}{4(1 - z/L_0)^2} - \frac{1}{4} + \frac{z}{L_0} \right) \quad (2.2)$$

Here F denotes the applied force, z the end-to-end distance of the DNA molecule, k_B the Boltzmann constant and T the absolute temperature. The effect of protein-DNA interactions on the DNA can be quantified by the fitting parameters L_p and L_0 from F - z curves of protein-DNA complexes.

The number of proteins that is bound to the DNA can be directly related to the change in end-to-end distance of the DNA molecule. Intercalation of a protein in the minor groove of the DNA that induces a bend in the DNA affects the end-to-end distance with a change in length Δz (Figure 2.1). This change in end-to-end distance is related to the force-dependent deflection length $\lambda(F) = \sqrt{k_B T \cdot L_p / F}$ as follows (191,192):

$$\Delta z = -\frac{1}{2} \lambda \cdot C(\alpha) \quad (2.3)$$

where L_p is the persistence length of bare DNA and $C(\alpha)$ is a geometric coefficient depending on the bending angle α :

$$C(\alpha) = 8 \left[1 - \cos\left(\frac{\alpha}{4}\right) \right] \quad (2.4)$$

Implementing the reduction of length Δz [Equation (2.3)] into the WLC [Equation (2.2)] and noting that $1/(4(1-z/L_0)^2) \gg z/L_0 - 1/4$ in our force regime, leads to a relation where the end-to-end distance (z) is directly related to the average number of proteins bound N_b (191,192):

$$\frac{z(F, N_b)}{L_0} \approx 1 - \frac{1}{2} \frac{\lambda(F)}{L_p} \left[1 + N_b \cdot C(\alpha) \frac{L_p}{L_0} \right] \quad (2.5)$$

This leads to an expression for the apparent persistence length, normalized by the number of proteins bound:

$$L_p^{app}(N_b) = \frac{L_p}{\left(1 + N_b \cdot \frac{L_p}{L_0} C(\alpha) \right)^2} \quad (2.6)$$

The number of proteins bound along single DNA molecules can now be determined by a model describing the mechanical response of DNA with multiple independent bends [Equation (2.6)]. It should be noted that this model only holds when the DNA is sufficiently stretched, such that the average distance between bound proteins is larger than the force-dependent deflection length, that is, $N_b \ll L_0 / \lambda$. In this force regime, bound proteins are distant enough to prevent the induced bends from interacting with each other. The aforementioned condition follows from an exact calculation that we performed for arbitrary linker lengths for a special case of protein arrangement (zigzag geometry). As for shorter linker lengths the end-to-end distance depends on the rotational setting of adjacent proteins, our aforementioned theory can lead to under- or overestimation of the number of bound proteins outside the allowed regime.

SUPPLEMENTARY INFORMATION

Geometry and energy of a kink formation

Consider a DNA chain under tension F with a protein adsorbed that causes a deflection α (see Figure 2.1). The energy of this chain is given by the sum of the bending and the potential energy:

$$E_{kink} = \int_0^{L_0} \left(\frac{A}{2} \dot{\theta}^2 - F \cos \theta \right) ds \quad (2.7)$$

Here $A = L_p k_B T$ is the bending modulus of the DNA chain, L_0 is its contour length, s gives the position along its contour, $0 \leq s \leq L_0$, and $\theta(s)$ is the angle between the tangent at position s and the force direction. The shape of the two sections of DNA chain to the left and to the right of the kink follow from the Euler-Lagrange equation $\ddot{\theta} = \lambda^{-2} \sin \theta$ with $\lambda = \sqrt{A/F}$.

In the following we extend the chain to $s = \mp\infty$ which introduces a negligible small error in the results as long as $\lambda \ll L_0$. The solution with the proper boundary conditions at the ends, namely $\theta(-\infty) = 0$ and $\theta(+\infty) = 2\pi$, is given by

$$\cos \theta(s) = 1 - \frac{2}{\cosh^2(s/\lambda)} \quad (2.8)$$

This solution features a single loop around $s = 0$. We cut out a segment of the solution from $-s_0 < s < s_0$ to obtain the geometry shown in Figure 2.1. The boundary condition at the protein-induced kink for e.g. the right arm is given by $\theta(s_0) = -\alpha/2$. The length loss due to the kink follows from

$$\Delta z = \int_{s_0}^{\infty} (\cos \theta(s) - 1) ds = 4\lambda (\tanh(s_0/\lambda) - 1) \quad (2.9)$$

Using $\theta(s_0) = \alpha / 2$ and trigonometric identities this can be rewritten as

$$\Delta z = -4\lambda(1 - \cos(\alpha / 4)) \quad (2.10)$$

From this follows directly Equation (2.5) and Equation (2.6). This result has already been reported earlier .

In addition, we calculate the energy associated with the formation of the kink, which is given by:

$$E_{\text{kink}} = A \int_{s_0}^{\infty} \dot{\theta}^2(s) ds - F\Delta z = \frac{4A}{\lambda^2} \int_{s_0}^{\infty} \frac{ds}{\cosh^2(s / \lambda)} - F\Delta z = 8\lambda F(1 - \cos(\alpha / 4)) \quad (2.11)$$

For the highest force, $F_{\text{max}} = 3.5$ pN , and the bending angle obtained from molecular dynamics (MD) simulations ($\alpha = \sim 46^\circ$, see Figure 2.3) this leads to the energy for kink formation $E_{\text{kink}} = 0.99 \cdot k_B T$.

Molecular dynamics simulations

The initial coordinates for protein-DNA complexes of Sul7 and Cren7 were taken from the co-crystal structures (PDB codes: 1BNZ for Sul7 (97) and 3LWH for Cren7 (101)). The SYBYL7.2 (Tripos Inc) generated ideal B-DNA duplex coordinates with identical sequence and length of the DNA from the co-crystal structures is used as the initial coordinates for the bare DNA simulation. All MD simulations were performed using CHARMM biomolecular simulation program (215) employing CHARMM22 all atom protein force field with CMAP corrections for proteins, and CHARMM27 all atom nucleic acid force field for nucleic acids (216-219). Missing hydrogens were added using HBUILD utility of CHARMM and allowed for 500 step steepest decent (SD) minimization on having harmonic constraints on heavy atoms. Later these systems were immersed in a cubic box with an edge length of 58 Å, treating the water using TIP3P model (220) and the water molecules within 2.4 Å distance of solute were deleted. All the crystal

water molecules were retained during the simulations. Sodium ions were placed randomly to make the systems electrically neutral. The bonds involving hydrogens were restrained by using SHAKE algorithm (221). Next, the systems were minimized using SD and Adopted Basis Newton Raphson (ABNR) methods up to 500 steps each with harmonic constraints on heavy atoms of protein and DNA. The systems were equilibrated for 100 ps with the same conditions. Particle mesh ewald summation method (222,223) was used to treat long-range interactions. CRYSTAL module, implemented in CHARMM, is used for periodic boundary conditions. All the simulations were performed in isobaric-isothermal (NPT) ensemble using the Nose-Hoover thermostat (224) for temperature control at 300 K and the Langevin piston algorithm (225) for constant pressure. The production simulations have been extended to 0.1 μ s with an integration time step of 2 fs using the Leapfrog integrator and the coordinates were saved for every 2 ps for further analysis.

The final 90 ns of the simulation trajectories were used for analysis using CHARMM and Curves+ (190) programs. All the translational and rotational motions were removed and only the systems with protein and DNA were considered by deleting the water and ions for this analysis. To assess the extent of bending in the DNA, roll parameters at the kink site region were calculated using Curves + (190).

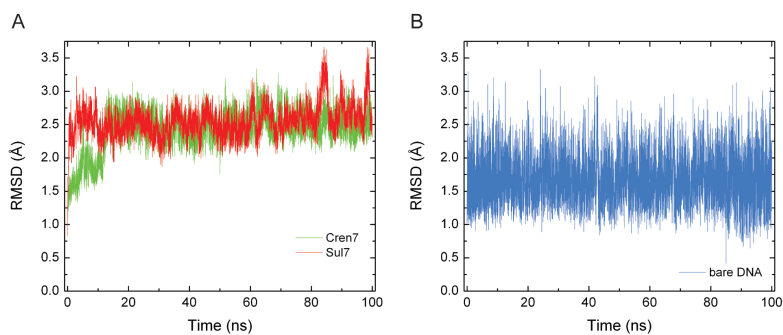


Figure S2.1 Root mean square deviations of MD simulations of **A.** Sul7-DNA and Cren7-DNA complexes and **B.** bare DNA

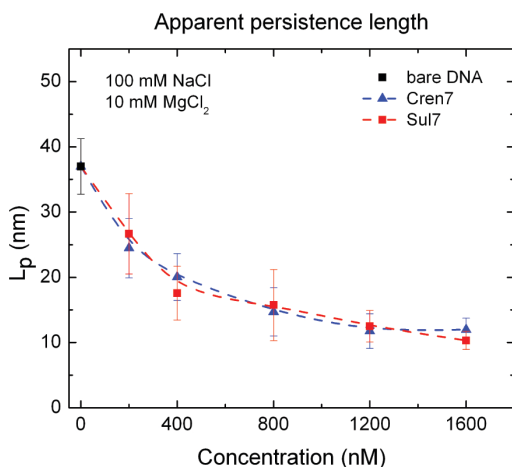


Figure S2.2 Apparent persistence length as a function of protein concentration in buffer containing mono- and divalent ions (100 mM NaCl and 10 mM MgCl₂). The persistence length decreases as a function of protein concentration at a higher protein concentration compared to experiments performed in buffer containing only 100 mM NaCl (see Figure 2.5 A).

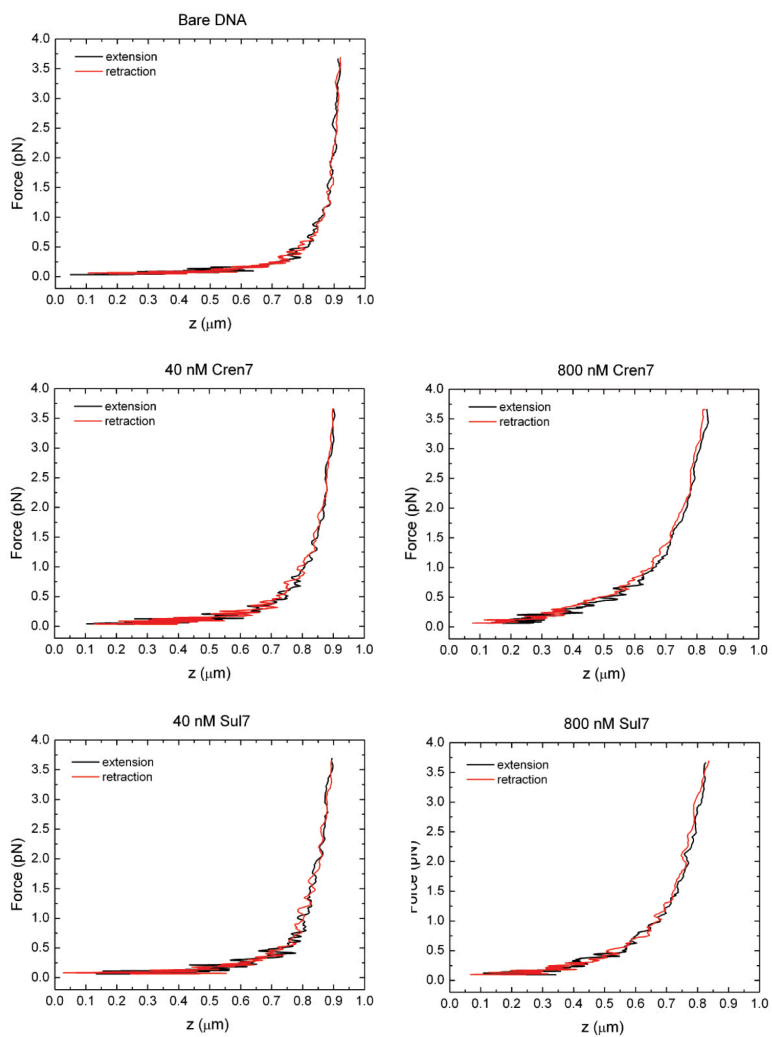


Figure S2.3 Force extension curves of bare DNA and protein-DNA complexes. The overlap of the extension and retraction curves shows that force extension curves are reversible, independent of the protein concentration.

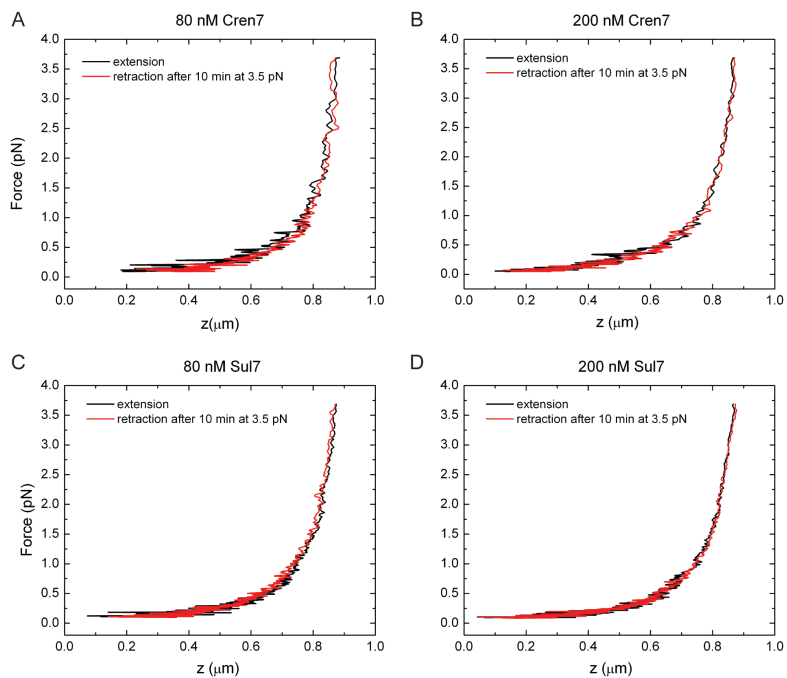


Figure S2.4 Force extension curves of protein-DNA complexes of long timescale experiments. The force extension curves are reversible even when holding the protein-DNA complexes at 3.5 pN for 10 minutes. This confirms that the proteins are bound stable to the DNA and do not dissociate within this timescale.

